

Use of Rejection Class to Enhance Airborne Imagery Classification

H.H. Bennett, Jr.¹, R.L. Campbell, Jr.¹, and N.H. Younan²

¹U.S. Army Corps of Engineers
Research and Development Center
Vicksburg, MS 39180

Telephone: (601) 634-3924 or (601) 634-4467

Fax: (601) 634-2732 or (601) 634-2301

E-mail: bennetj2@wes.army.mil or campber1@wes.army.mil

²Department of Electrical and Computer Engineering
Box 9571

Mississippi State University
Mississippi State, MS 39762

Telephone: (662) 325-3721

Fax: (662) 325-2298

E-mail younan@ece.msstate.edu

Abstract

The performance of a prior classification work is enhanced by introducing a rejection class that accurately describes a particular source of false alarm. Success of this enhancement is measured by observing changes in the Receiver Operating Characteristic (ROC) curves corresponding to two different fixed strengths of the rejection class. Source data is taken from airborne imagery collected by a line-scanner system known as REMIDS (REMOte IDentification System) through funding from the Environmental Security Technology Certification Program (ESTCP).

1. Introduction

In collecting the data, the REMIDS system [1] was mounted on a UH-60A Blackhawk Helicopter, as shown in Figure 1, and was flown at an altitude of 130 feet and at a forward velocity of 32.5 knots to achieve a comprehensive data set for land areas suspected of containing unexploded ordnance. Two distinct channels, parallel and cross polarization, were provided by an active laser, and a third channel used to determine temperature was provided by a passive infrared line-scanner. The two active laser channels were transformed to provide

processed polarization and reflectance channels, which were combined with the temperature channel to yield a 3-D total feature space. Assuming a value range of 0 to 255, the following four classes [2] were used to detect man-made and man-processed materials from the airborne imagery. The angular brackets indicate the mean, and the weighted standard deviations are denoted by σ_w .



Figure 1. REMIDS/Black Hawk Interface

Material	$\langle P \rangle$	$\sigma_P W_P$	$\langle R \rangle$	$\sigma_R W_R$	$\langle T \rangle$	$\sigma_T W_T$
Oxidized Iron and olive drab paint	225	40	50	30	100	40
White paint	200	35	140	40	90	40
Aluminum	255	40	130	40	20	50
Dielectric mines (white plastic)	25	30	130	40	100	35

Table 1. Material Parameters

Given the polarization (P), reflectance (R), and temperature (T) for each pixel, classification was performed via the following distance equation [4,6]:

$$D_i = \sqrt{\left(\frac{P - \langle P_i \rangle}{\sigma_{P_i} W_{P_i}}\right)^2 + \left(\frac{R - \langle R_i \rangle}{\sigma_{R_i} W_{R_i}}\right)^2 + \left(\frac{T - \langle T_i \rangle}{\sigma_{T_i} W_{T_i}}\right)^2},$$

where i denotes the i^{th} classification test. By setting a global threshold distance, each pixel was classified into one of five categories: the four above and a "background" category. The "background" category was declared if the distance for all four-classification tests was larger than the global threshold distance.

In the initial work, the classification results, obtained by the above procedure, produced an undesirable number of false alarms in the iron/olive drab paint class, because of a naturally occurring material known as desert varnish. Therefore, this subsequent investigation focuses on the creation of a desert varnish class in an attempt to isolate and eliminate the adverse effects of this highly pronounced terrain artifact.

2. Investigation

Imagery of an area known to contain substantial amounts of desert varnish [2,3] was analyzed in terms of the mean and variance of the three feature space channels, yielding the following class description:

Material	$\langle P \rangle$	σ_P	$\langle R \rangle$	σ_R	$\langle T \rangle$	σ_T
Desert varnish	180	17	72	8	103	14

Table 2. Desert Varnish Parameters

For the investigation, the mean integrities were maintained, but the standard deviations were weighted to modify the distance calculation effects of the three individual channels. The first and second core strengths of the desert varnish class were defined as follows:

Strength	$\sigma_P W_P$	$\sigma_R W_R$	$\sigma_T W_T$
1	30	30	70
2	25	25	50

Table 3. Rejection Class Strengths

For each strength, the desert varnish class was included with the standard four classes, and the global threshold distance was swept from 0.7 to 1.7 to yield the detection curves in Figures 2 and 3. The intermediate steps include

1. applying a six category classification test (the five classes plus a "background" class) to each pixel,
2. assigning all desert varnish pixels to the "background",
3. determining the centroid and the major and minor axes of any distinctive collection of "non-background" adjoining or pseudo-adjoining pixels,
4. determining for each set of grouped pixels if the aggregate shape-measures constitute a target,
5. and finally, comparing the target identification results to the results obtained by a physical walkthrough of the analyzed area.

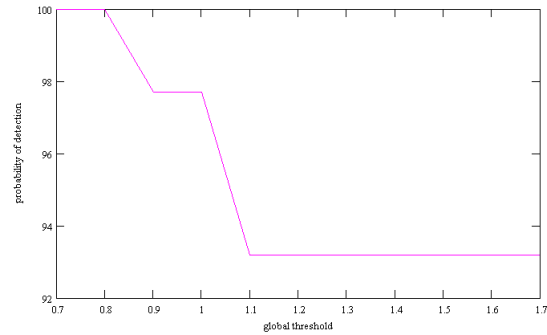


Figure 2. Probability of Target Detection Versus Threshold Distance for Strength 1.

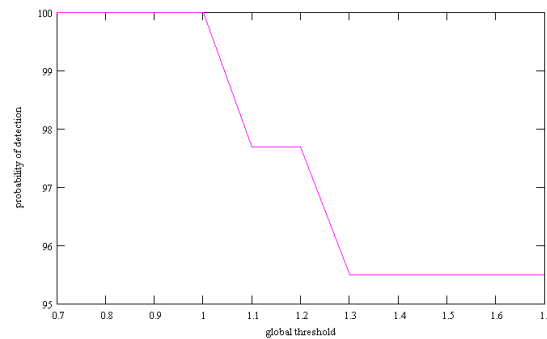


Figure 3. Probability of Target Detection Versus Threshold Distance for Strength 2.

The resulting curves were used to determine the maximum threshold distance that maintained 100%

detection. Respective of the desert varnish strengths, $\max\{d_{REJECTION}\} = 0.8$ and 1.0 . With the rejection distance fixed to its maximum value, the above enumerated procedure was repeated for both rejection class strengths, yielding Figures 4 and 5.

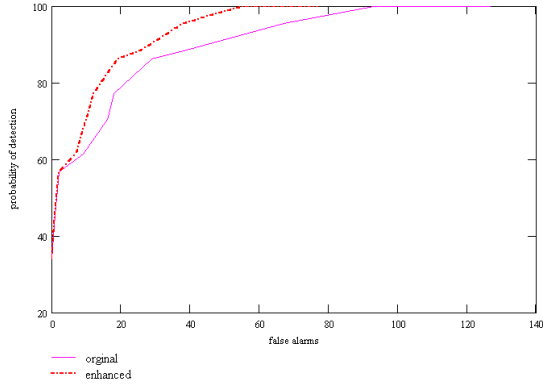


Figure 4. Original and Rejection Class Strength 1 ROC curves.

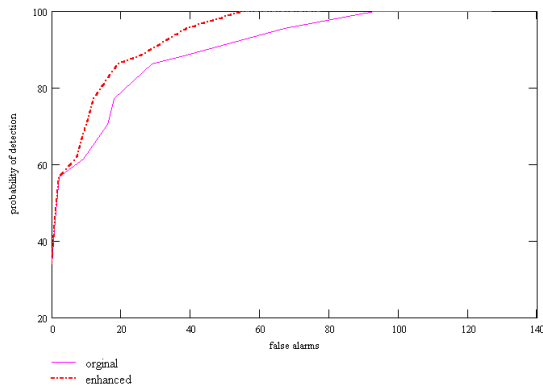


Figure 5. Original and Rejection Class Strength 2 ROC curves.

Since applying a rejection class is often an afterthought, the analysis was modified in lieu of the pixel information being available only near the target centroids. The enumerated procedure includes

1. for a given window size, classifying all windowed pixels using a six category classification such that the window center coincides with the target centroid,
2. using a popularity filter [5] (one that selects the window mode) to classify the target,
3. rejecting the target if it is classified as desert varnish,
4. and finally, comparing the target identification results to the walkthrough results.

Three window sizes (1x1, 3x3, and 5x5) were used to obtain Figures 6-9, where, respective of the two different rejection class strengths, Figures 6 and 7 are detection

curves used to find $\max\{d_{REJECTION}\}$ and Figures 8 and 9 contain ROC curves for the three window sizes.

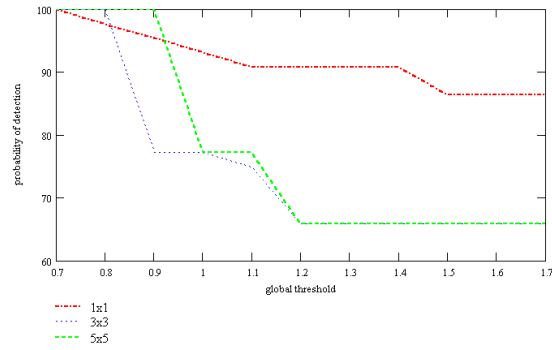


Figure 6. Probability of Target Detection After Windowed Rejection versus Global Threshold Distance for Rejection Class Strength 1.

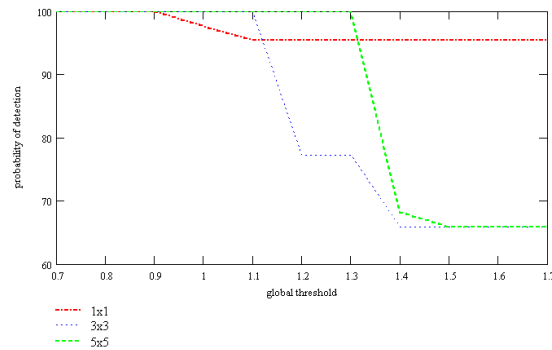


Figure 7. Probability of Target Detection After Windowed Rejection versus Global Threshold Distance for Rejection Class Strength 2.

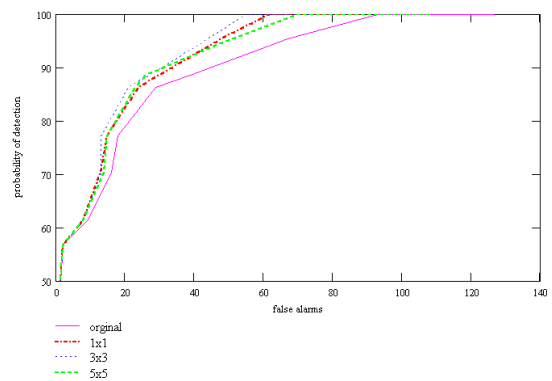


Figure 8. Original ROC Curve and Rejection Class Strength 1 Windowed Rejection ROC Curves.

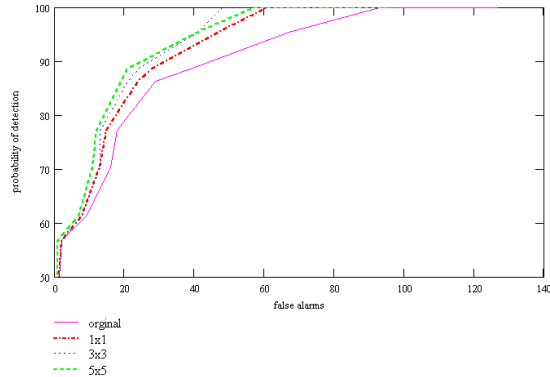


Figure 9. Original ROC Curve and Rejection Class Strength 2 Windowed Rejection ROC Curves.

3. Results

As seen by viewing the ROC curves for all cases, the introduction of a rejection class has clearly improved the classification process. One might contend that this success is highly contingent upon the proper selection of $\max\{d_{REJECTION}\}$, which cannot be identified without thorough a priori knowledge of all individual targets in a region. However, setting $\max\{d_{REJECTION}\}$ can be achieved by analyzing a calibration site that is statistically indicative of the one to be tested. If a calibration site is not available, varying this parameter will likely provide strong clues as to the true classification of a flagged target, simply by the target's classification response to the variation.

The difference in ROC curves for the two desert varnish class strengths was nominal as expected, since the stronger rejection class consistently required a smaller fixed threshold distance. The results for the different window sizes did not follow a definitive trend since different geometric nuances had unique effects on the different windowed rejection results, therefore weakening their distinction.

4. Conclusions

Given a statistically measurable background material that is known to lie near a bona fide class, the careful construction of a material rejection class may remove many of the adverse classification effects introduced by the material.

References

1. John H. Ballard, R. M. Castellane, B. H. Miles, and K. G. Wesolowicz, "The Remote Minefield Detection System (REMIDS) II major components and operation," US Army Engineer Waterways Experiment Station Technical Report, 1992.
2. Hollis H. Bennett, Jr., Thomas W. Altshuler, Lias Porter, Frank Rotondo, and Dave Sparrow, "Independent analysis of detection data for unexploded ordnance from the Remote Identification System (REMIDS)," UXO Forum Proceedings, 1998.
3. Hollis H. (Jay) Bennett and Kelly Rigano, "Surface unexploded ordnance detection via an active/passive multispectral line scanner system at Yuma Proving Ground, Arizona," UXO Forum Proceedings, 1997.
4. R. O. Duda and P. E. Hart, *Pattern Classification and Scene Analysis*, John Wiley & Sons, NY, 1973.
5. J. D. Foley, A. Van Dam, and S. K. Feiner, J. F. Hughes, *Computer Graphics: Principles and Practices*, 2nd ed., Addison-Wesley, 1990.
6. Robert J. Schalkoff, *Pattern Recognition: Statistical, Structural and Neural Approaches*, John Wiley & Sons, NY, 1992.